Journal of Information Systems and Telecommunication
Vol.10, No.2, April-June 2022, 132-140
http://jist.acecr.org
ISSN 2322-1437 / ESSN:2345-2773

Defect Detection using Depth Resolvable Statistical Post Processing in Non-Stationary Thermal Wave Imaging

G.V.P. Chandra Sekhar Yadav[1,2*], V.S. Ghali[1], Naik. R. Baloji[3]

[1].Infrared Imaging Center, Department of ECE, Koneru Lakshmaiah Education Foundation, A.P, Vaddeswaram, India
[2].Department of ECE, DVR & Dr HS MIC College of Technology, Kanchikacherla, A.P, India
[3].Naval Materials Research Laboratory, Ambernath (E), Dist. Thane, Maharashtra, 421506 India

Received: 31 Jan 2021/ Revised: 25 Oct 2021/ Accepted: 05 Dec 2021
DOI:

Abstract

Defects that are generated during various phases of manufacturing or transporting limit the future applicability and serviceability of materials. In order to detect these defects a non-destructive testing modality is required. Depth resolvable subsurface anomaly detection in non-stationary thermal wave imaging is a vital outcome for a reliable prominent investigation of materials due to its fast, remote and non-destructive features. The present work solves the 3-Dimensional heat diffusion equation under the stipulated boundary conditions using green's function based analytical approach for recently introduced quadratic frequency modulated thermal wave imaging (with FLIR SC 655A as infrared sensor with spectral range of 7.5-14µm and 25 fps) to explore the subsurface details with improved sensitivity and resolution. The temperature response obtained by solving the 3-Dimensional heat diffusion equation is used along with random projection-based statistical post-processing approach to resolve the subsurface details by imposing a band of low frequencies (0.01-0.1 Hz) over a carbon fiber reinforced polymer for experimentation and extracting orthonormal projection coefficients to improve the defect detection with enhanced depth resolution. Orthonormal projection coefficients are obtained by projecting the orthonormal features of the random vectors that are extracted by using Gram-Schmidt algorithm, on the mean removed dynamic thermal data. Further, defect detectability of random projection-based post-processing approach is validated by comparing the full width at half maxima (FWHM) and signal to noise ratio (SNR) of the processed results of the conventional approaches. Random projection provides detailed visualization of defects with 31% detectability even for deeper and small defects in contrast to conventional post processing modalities. Additionally, the subsurface anomalies are compared with their sizes based on full width at half maxima (FWHM) with a maximum error of 0.99% for random projection approach.

Keywords: Non-Stationary Thermal Wave Imaging (NSTWI); Fast Fourier Transform (FFT); Correlation; Random Projection Transform (RPT).

1- Introduction

Subsurface analysis for non-stationary thermal wave imaging (NSTWI) gaining importance from the past decades due to its distinct wide, fast, non-invasive and remote testing properties. Different processing techniques are available to get the hidden features of the material. Out of them, the conventional phase approach is mostly used due to reduced non-uniform emissivity and radiation. Even though the conventional phase-based analysis gives the subsurface details, but it is not used to get deeper details due to its limited frequency resolution. This paper focuses on the recently introduced depth resolvable post-processing approach to provide fine subsurface details with improved frequency resolvable NSTWI technique.

Active infrared thermography is one of the non-destructive testing (NDT) methods to test the integrity of the material,[1] without impairing its future utility. In active infrared thermography, subsurface analysis is done by comparing the thermal response obtained by variations in thermophysical properties of diffused waves at anomalies of different depths. Pulse thermography (PT), lock-in thermography (LT), pulse phase thermography (PPT) and non-stationary thermography are various techniques of active thermography classified on the employment of optical input.

A large power rectangular input with less duration is used to test the integrity of the object in PT,[2] but the obligation of more power along with non-uniform effects limits it. In

✉ **G.V.P. Chandra Sekhar Yadav**
sekhar.yadav2008@gmail.com

LT, a mono frequency continuous sinusoidal stimulus with small peak is used for investigation and phase-based analysis is performed to get the subsurface details. Limited depth resolution with mono frequency input stimulus,[3] causes repetitive experimentation in LT. In PPT, a similar stimulus is applied as in PT and phase analysis is done to get the subsurface details like LT to reduce the non-uniform effects; yet the obligation of more power [4] remained as a constraint of conventional thermographic approaches. Thus, NSTWI is introduced to test the integrity of the object with low power non-stationary stimulus in single experimentation.[5, 6, 7, 8, 9, 10, 11, 12]

In 2006, R. Mulaveesala introduced linear frequency modulated thermal wave imaging (LFMTWI),[5] which uses a low power continuous band of low frequency modulated chirped stimulus to test the object with moderate depth resolution. Later V.S. Ghali introduced its quadratic version called quadratic modulated thermal wave imaging (QFMTWI) in 2012,[6] by imposing a continuous band of low quadratic frequency-modulated chirped stimulus over the object with improved depth resolvable capability.

In the conventional phase approach, a fast fourier transform (FFT) with the orthogonal basis of multiple frequencies is applied on every thermal profile, later their relative phase value is extracted to discriminate,[7] the defective and non-defective regions. Pulse compression (PC) uses a matched filter-based cross-correlation approach and corresponding peak delays,[8, 9] are used to characterize defective and non-defective regions. In the Random projection transform (RPT) approach, high-dimensional data can be subsampled using the Johnson-Lindenstrauss lemma, while maintaining its maximum features by projecting,[10] on a smaller number of orthonormal random basis vectors with less complexity.

This work uses QFMTWI for experimental investigation of carbon fiber reinforced polymer (CFRP). Later, RPT based post-processing technique uses the coefficients of orthonormal projection to discriminate the defective and non-defective regions of the test object. This paper validates the defect detection capability of RPT technique by considering full width at half maxima (FWHM) and signal to noise ratio (SNR) and comparing them with conventional FFT and PC.

2- Theory of Thermal Waves

The temperature response on the surface of the material has been obtained by solving the 3-D heat equation by considering internal heat generation Q_m. The mathematical model is obtained by using Greens function under the Neumann boundary conditions.[11] Consider 3-D diffusion Eq. (1)

$$\frac{\partial^2 T(x,y,z,t)}{\partial^2 x}+\frac{\partial^2 T(x,y,z,t)}{\partial^2 y}+\frac{\partial^2 T(x,y,z,t)}{\partial^2 z}=\frac{1}{\alpha}\frac{\partial T(x,y,z,t)}{\partial t}+Q_m \quad (1)$$

Where α refers the thermal diffusivity of the test specimen. The solution is acquired by resolving the homogeneous section of Eq. (2) using variable separable method and it can be written as

$$T(x,y,z,t)=X(x)Y(y)Z(z)\Gamma(t) \quad (2)$$

By substituting Eq. (2) in Eq. (1)

$$\frac{\partial^2 (X(x)Y(y)Z(z)\Gamma(t))}{\partial^2 x}+\frac{\partial^2 (X(x)Y(y)Z(z)\Gamma(t))}{\partial^2 y}$$

$$+\frac{\partial^2 (X(x)Y(y)Z(z)\Gamma(t))}{\partial^2 z}=\frac{1}{\alpha}\frac{\partial X(x)Y(y)Z(z)\Gamma(t))}{\partial t} \quad (3)$$

$$\frac{Y(y)Z(z)\Gamma(t)\partial^2 X(x)}{\partial^2 x}+\frac{X(x)Z(z)\Gamma(t)\partial^2 Y(y)}{\partial^2 y}$$

$$+\frac{X(x)Y(y)\Gamma(t)\partial^2 Z(z)}{\partial^2 z}=\frac{1}{\alpha}\frac{X(x)Y(y)Z(z)\partial\Gamma(t)}{\partial t} \quad (4)$$

Divide with $X(x)Y(y)Z(z)\Gamma(t)$ on both sides

$$\frac{X^{''}(x)}{X(x)}+\frac{Y^{''}(y)}{Y(y)}+\frac{Z^{''}(z)}{Z(z)}=\frac{1}{\alpha}\frac{\Gamma^{'}(t)}{\Gamma(t)} \quad (5)$$

Let

$$\frac{X^{''}(x)}{X(x)}=-\beta^2;\frac{Y^{''}(y)}{Y(y)}=-\gamma^2;\frac{Z^{''}(z)}{Z(z)}=-\eta^2;\frac{\Gamma^{'}(t)}{\Gamma(t)}=-\lambda^2 \quad (6)$$

Put Eq. (6) in Eq. (5), we get

$$\lambda^2=\alpha(\beta^2+\gamma^2+\eta^2) \quad (7)$$

Since the solutions are negative

$$X(x)=A_1\cos\beta x+B_1\sin\beta x$$

$$Y(y)=A_2\cos\gamma y+B_2\sin\gamma y$$

$$Z(z)=A_3\cos\eta z+B_3\sin\eta z$$

$$\Gamma(t)=Ce^{-\alpha(\beta^2+\gamma^2+\eta^2)t} \quad (8)$$

Substitute Eq. (8) in Eq. (2)

$$T(x,y,z,t)=(A_1\cos\beta x+B_1\sin\beta x)$$

$$(A_2\cos\gamma y+B_2\sin\gamma y)(A_3\cos\eta z+B_3\sin\eta z)$$

$$Ce^{-\alpha(\beta^2+\gamma^2+\eta^2)t} \quad (9)$$

Boundary conditions and initial conditions are

$$-k\frac{\partial T}{\partial x}\Big|_{x=0}=Q_T(t);-k\frac{\partial T}{\partial x}\Big|_{x=a}=0;$$

$$-k\frac{\partial T}{\partial y}\Big|_{y=0,b}=0;$$

$$-k\frac{\partial T}{\partial z}\Big|_{z=0,c}=0;$$

$$T(x,y,z,0)=T_0; \quad (10)$$

Where $Q_T(t)$ is the combination of DC and QFM chirp signal i.e., $Q_T(t)=1+Q(t)$

Q(t) is the QFM chirp signal; 1 is the DC added to QFM to overcome the simultaneous heating and cooling phase of experimentation $Q_T(t) = Q_0\left(1+e^{j2\pi(f_0+b_0t^2)t}\right); x=0$

Where, Q_0 refers constant heat flow, f_0 refers starting frequency and b_0 refers the chirp rate of the incident QFM chirp signal. Fig. 1 represents the DC added QFM chirp signal of 2kw power at 0.01-0.1Hz frequency.

By substituting Eq. (10) in Eq. (9), we get solution for Greens function for Eq. (1) [11]

$$G(x,y,z,t;\varepsilon,\xi,\delta,\tau) = \frac{R_1R_2R_3}{abc}\sum_{m=0}^{\infty}\sum_{n=0}^{\infty}\sum_{p=0}^{\infty}\cos\beta_m x\cos\beta_m\varepsilon\cos\gamma_n y\cos\gamma_n\xi\cos\eta_p z\cos\eta_p\delta e^{-\alpha(\beta_m^2+\gamma_n^2+\eta_p^2)(t-\tau)} \quad (11)$$

$$\beta_m = \frac{m\pi}{a}; m = 0,1,2....\infty$$

$$\gamma_n = \frac{n\pi}{b}; n = 0,1,2....\infty$$

$$\eta_p = \frac{p\pi}{c}; p = 0,1,2....\infty$$

Where

$$R_1 = \begin{cases}1; m=0\\2; m=1,2.....\infty\end{cases}$$

$$R_2 = \begin{cases}1; n=0\\2; n=1,2.....\infty\end{cases}$$

$$R_3 = \begin{cases}1; p=0\\2; p=1,2.....\infty\end{cases}$$

In terms of Greens function the solution for Eq. (1) which refers non-homogeneous heat diffusion is given as

$$T(x,y,z,t) = \frac{\alpha}{k}\int_0^t\int_0^a\int_0^b\int_0^c Q_m G(x,y,z,t;\varepsilon,\xi,\delta,\tau)d\delta d\xi d\varepsilon d\tau - \alpha\int_0^t\int_0^b\int_0^c T(\varepsilon,\xi,\delta,\tau)\nabla_j G(x,y,z,t;\varepsilon,\xi,\delta,\tau)d\delta d\xi + \alpha\int_0^t\int_0^b\int_0^c G(x,y,z,t;\varepsilon,\xi,\delta,\tau)\nabla_j T(\varepsilon,\xi,\delta,\tau)d\delta d\xi + \int_0^a\int_0^b\int_0^c T(\varepsilon,\xi,\delta,0)G(x,y,z,t;\varepsilon,\xi,\delta,0)d\delta d\xi d\varepsilon \quad (12)$$

$$T(x,y,z,t) = \frac{\alpha}{k}\int_0^t\int_0^a\int_0^b\int_0^c Q_m G(x,y,z,t;\varepsilon,\xi,\delta,\tau)d\delta d\xi d\varepsilon d\tau + \alpha\int_0^t\int_0^b\int_0^c G(x,y,z,t;0,\xi,\delta,\tau)\frac{\partial T(0,\xi,\delta,\tau)}{\partial x}d\delta d\xi d\tau - \alpha\int_0^t\int_0^b\int_0^c G(x,y,z,t;a,\xi,\delta,\tau)\frac{\partial T(a,\xi,\delta,\tau)}{\partial x}d\delta d\xi d + \int_0^a\int_0^b\int_0^c T(\varepsilon,\xi,\delta,0)G(x,y,z,t;\varepsilon,\xi,\delta,0)d\delta d\xi d\varepsilon \quad (13)$$

Apply the boundary conditions and initial conditions from Eq. (10) to above Eq. (13), we get

$$T(x,y,z,t) = \frac{\alpha}{k}\int_0^t\int_0^a\int_0^b\int_0^c Q_m G(x,y,z,t;\varepsilon,\xi,\delta,\tau)d\delta d\xi d\varepsilon d\tau - \frac{\alpha}{k}\int_0^t\int_0^b\int_0^c G(x,y,z,t;0,\xi,\delta,\tau)Q_T(\tau)d\delta d\xi d\tau + \int_0^a\int_0^b\int_0^c T(\varepsilon,\xi,\delta,0)G(x,y,z,t;\varepsilon,\xi,\delta,0)d\delta d\xi d \quad (14)$$

In the case of experimentation $Q_T(t)$ is considered as the combination of DC and QFM chirp signal to overcome the simultaneous heating and cooling process.

After the experimentation while doing the qualitative analysis, DC response was removed as it doesn't contain any information.

Hence the final temperature equation can be obtained from Eq. (14) is

$$T(x,y,z,t) = -\frac{\alpha}{k}\int_0^t\int_0^b\int_0^c G(x,y,z,t;0,\xi,\delta,\tau)Q(\tau)d\delta d\xi d\tau \quad (15)$$

By substituting Greens function from Eq. (11) the above Eq. (15) can be written as

$$T(x,y,z,t) = -\frac{\alpha}{k}\int_0^t\int_0^b\int_0^c \frac{R_1R_2R_3}{abc}\sum_{m=0}^{\infty}\sum_{n=0}^{\infty}\sum_{p=0}^{\infty}\cos\beta_m x\cos\gamma_n y\cos\gamma_n\xi\cos\eta_p z\cos\eta_p\delta e^{-\alpha(\beta_m^2+\gamma_n^2+\eta_p^2)(t-\tau)}Q(\tau)d\delta d\xi d\tau \quad (16)$$

$$T(x,y,z,t) = -\frac{\alpha}{k}\int_0^t\frac{R_1}{a}\sum_{m=0}^{\infty}\cos\beta_m x e^{-\alpha(\beta_m^2)(t-\tau)}Q(\tau)d\tau \quad (17)$$

$$T(x,y,z,t) = -\frac{\alpha}{ka}\int_0^t\left(1+2\sum_{m=1}^{\infty}\cos\beta_m x e^{-\alpha(\beta_m^2)(t-\tau)}\right)Q(\tau)d\tau \quad (18)$$

By considering m=0 and 1 and neglecting higher order m values because

$\cos\beta_m x = 1; m = 0,1,2,3....\infty$ for $a = 0.005m$

$$e^{-\alpha(\beta_m^2)(t-\tau)} = e^{-0.42*10^{-6}\left(\frac{m\pi^2}{25*10^{-6}}\right)(t-\tau)}$$

$=1$;m=0

$=0.84$;$m=1$

$=0.515$;$m=2$

$=0.22$;$m=3$

$=0.07$;$m=4$

$=0.015$;$m=5$

$=0.002$;$m=6$

$=0.0002$;$m=7$

$=0.00002$;$m=8$

On the application of Laplace transform, we get

$$T(X,Y,Z,s) = -\frac{\alpha}{ka}\frac{Q(s)}{s} + \frac{2\alpha\cos\beta_m x}{ka}\int_0^t \left(\sum_{m=1}^{\infty} e^{-\alpha(\beta_m^2)(t-\tau)}\right) Q(\tau)d\tau$$

$$T(X,Y,Z,s) = -\frac{\alpha}{ka}\frac{Q(s)}{s} + \frac{2\alpha\cos\left(\frac{\pi}{a}x\right)}{ka}\int_0^t e^{-\frac{\alpha(\pi^2)(t-\tau)}{a^2}} Q(\tau)d\tau$$

$$T(X,Y,Z,s) = -\frac{\alpha}{ka}\frac{Q(s)}{s} + \frac{2\alpha\cos\left(\frac{\pi}{a}x\right)}{ka}\frac{e^{-\frac{\alpha\pi^2 t}{a^2}} Q\left(s-\frac{\alpha\pi^2}{a^2}\right)}{s} \quad (19)$$

Where Q(s) refers the Laplace transform of Q(t) at x=0, α is thermal diffusivity of the test sample, k refers the thermal conductivity of the material and a is the length in x-direction respectively. Further, the obtained thermal response is analyzed by different processing algorithms to get the detail visualization.

3- Experimentation

Experimentation was conducted on CFRP sample to validate the proposed RPT technique. Fig. 2 represents the layout of CFRP sample used for testing.

Experimental CFRP specimen of dimensions 24x24x0.5cm with 36 artificially created circular back-holes with various sizes located at various depths (Fig. 2) is energized with a quadratic modulated chirped stimulus for a 0.01-0.1Hz band of low frequencies (Fig. 1) for duration of 100s. The experimental setup shown in Fig. 3 is explained as follows: the experimental side of the object to be tested is placed opposite to the IR camera, the input excitation is applied over the object with a set of halogen lamps placed opposite to the test object [11] and the entire set up is controlled by using a control unit, an IR camera is used to capture the thermal perturbations of the test object simultaneously and later exported to processing unit for further subsurface analysis.

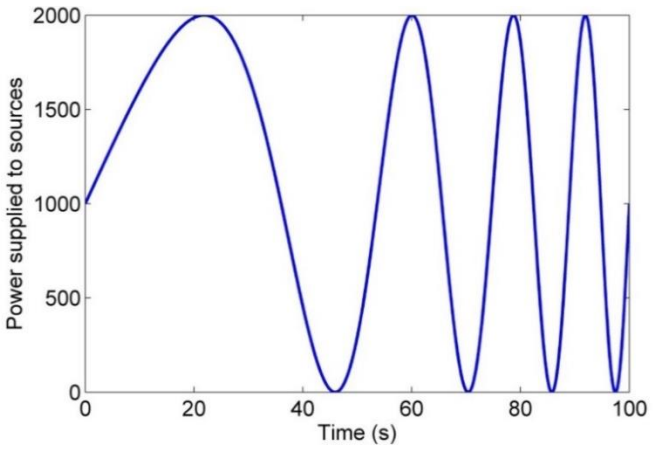

Fig. 1 Schematic of incident quadratic frequency-modulated heat flux of 2kw power at 0.01-0.1Hz frequency

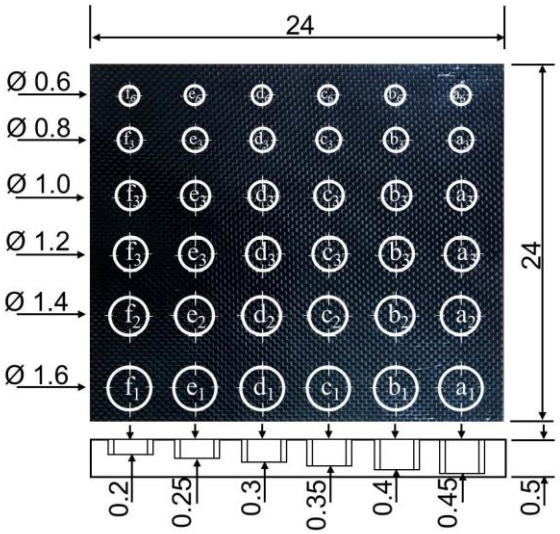

Fig. 2 CFRP specimen layout (dimensions in cm)

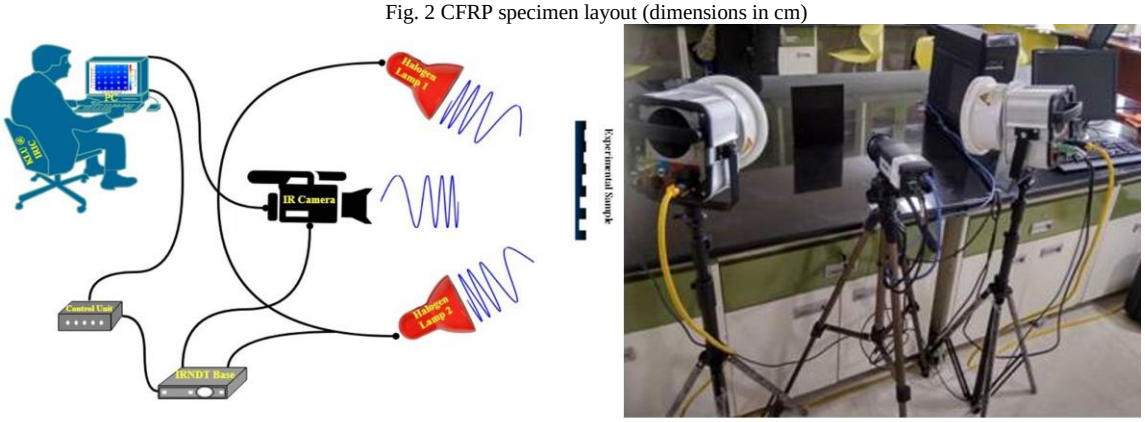

a b

Fig. 3 a. Schematic view and b. Experimental set up of QFMTWI

4- Results and Discussions

The captured thermal response using IR camera consists of both static, dynamic responses [12] by considering DC in the input excitation (Fig. 1). The static response doesn't contain any information regarding subsurface details; it must be pre-processed before processing through various processing algorithms [13]. Hence the static response was removed by using a suitable linear fitting algorithm; the mean removed dynamic response is processed using FFT, PC and RPT techniques to get detailed visualization of subsurface layers is shown in Fig. 4.

4-1- FFT

FFT is the widely used conventional post-processing technique [14, 15] for defect characterization in NSTWI. In this, FFT is applied over each profile as in Eq. (20) of mean removed dynamic thermal response and corresponding phase value is extracted using Eq. (21) and placed in their respective locations [16] to construct the phase grams.

$$F(w)=\sum_{n=0}^{N-1} f(n)e^{jwn} \tag{20}$$

$$\phi_{FFT}=\tan^{-1}\left(\frac{\mathrm{Im}(F(nw))}{\mathrm{Re}(F(nw))}\right) \tag{21}$$

Further phase contrast is calculated to characterize [17] the defective and non-defective regions.

4-2- PC

PC is the correlation based matched filter technique, which cross-correlates the referenced non-defective thermal profile with each profile of the mean removed thermal response [18, 19, 20] using Eq. (22). The corresponding normalized correlation coefficients are placed accordingly to construct correlation images.

$$g(\tau)=\int_{-\infty}^{+\infty} s(t)h(t+\tau)dt \quad (22)$$

Normalized correlation contrast discriminates defective and non-defective regions. Normalized peak delays between the reference correlation profile with defective profiles are used [21] to characterize the subsurface details. Fig. 5 shows the normalized correlation peak delays of reference compressed profile and defective compressed profiles of 1.6cm diameter (defects a_1 to f_1) and corresponding peak delay vs. depth plot. The decreased normalized correlation peak delay value from deeper defect (f_1) to shallowest defect (a_1) discriminates the depth of the defects.

4-3- RPT

In RPT, the orthonormal features of the random vectors are extracted by using the Gram-Schmidt algorithm and later the mean removed dynamic thermal profiles are projected on these vectors to get the normalized random projection coefficients [22]. The random vectors in the orthonormal basis are generated by extracting Eq. (23)

$$V_1=\frac{f_1[n]}{|f_1[n]|};V_2=f_2[n]-(V_1^T f_2[n])V_1 \quad (23)$$

The entire procedure is repeated for each random vector and then mean removed dynamic thermal profiles are projected on them. In this, the three-dimensional mean removed dynamic thermal data is converted into two-dimensional data and later this two-dimensional dynamic data is projected on the random vectors generated by using the Gram-Schmidt algorithm [23]. Further, the random projected coefficients are used to discriminate the anomalies and rearranged to get the random projected images.

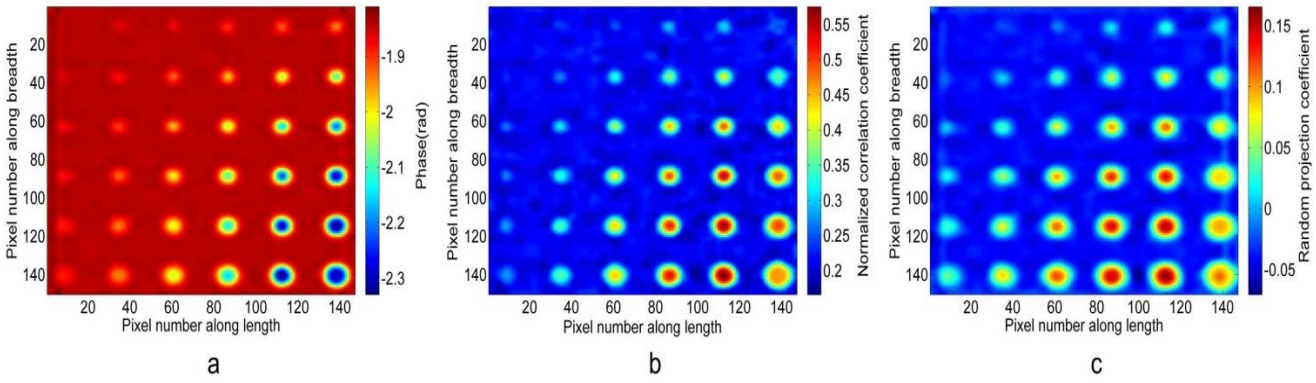

Fig. 4 Processed results of CFRP sample for QFMTWI a. FFT phase at 0.05Hz, b. Correlation image at 7.8s and c. Random projection image at 4th component

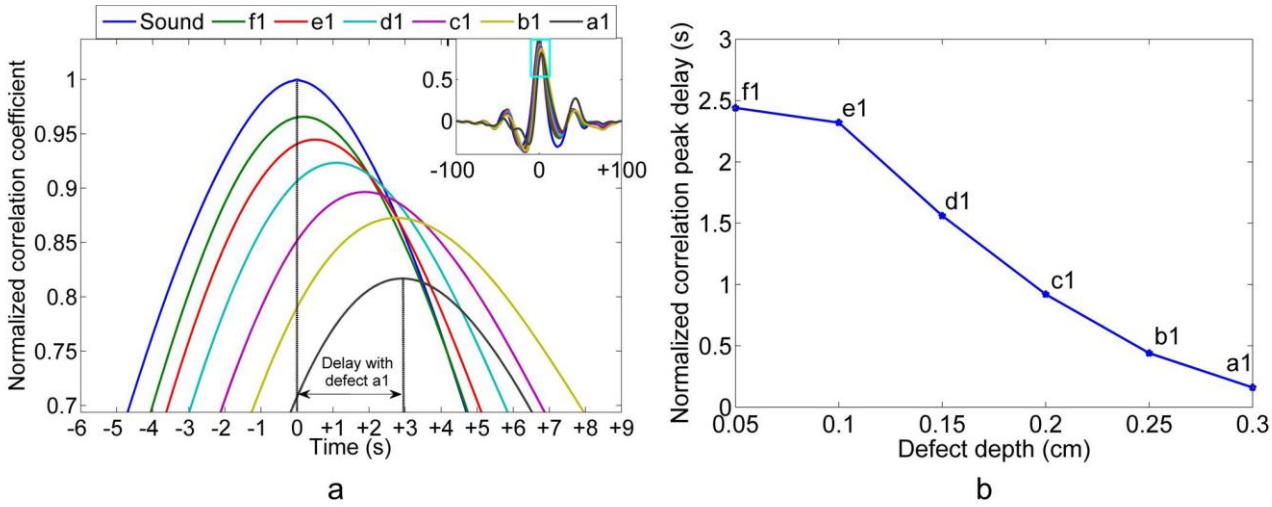

Fig. 5 a. Enlarged (of inset) normalized correlation peak delays of reference and defective profiles of 1.6cm diameter and b. Corresponding peak delay vs. depth of the defect

4-4- SNR

Defect detectability of the processing method is explained by estimating SNR [24, 25] using Eq. (24)

$$SNR = 20\log\left(\frac{\mu_{defective} - \mu_{non-defective}}{\sigma_{non-defective}}\right) \quad (24)$$

Fig. 6 compares the SNR of each defect of the RPT approach with the conventional FFT and PC based approaches. From Fig. 6, it shows that the RPT based post-processing approach detects the defects better than conventional approaches in terms of SNR.

4-5- FWHM

The qualitative subsurface analysis is done by estimating the size of defects, for this a widely used thermographic performance metric [26] FWHM is computed and estimated defect diameters are shown in the following table 1. Table 1 compares the actual diameter of the defects with estimated FWHM for processed results and its corresponding error values. RPT based post-processing approach gives the nearest diameters of the defects than the conventional approaches.

The result analysis authenticates, that the proposed RPT based statistical approach through 3D green's function analytical analysis detects the deeper and smaller defects with improved sensitivity and resolution by making use of randomly generated orthonormal vectors to discriminate the defective area with sound area and it is validated experimentally for CFRP sample using QFMTWI. To support this SNR and FWHM are calculated and compared with conventional signal processing approaches.

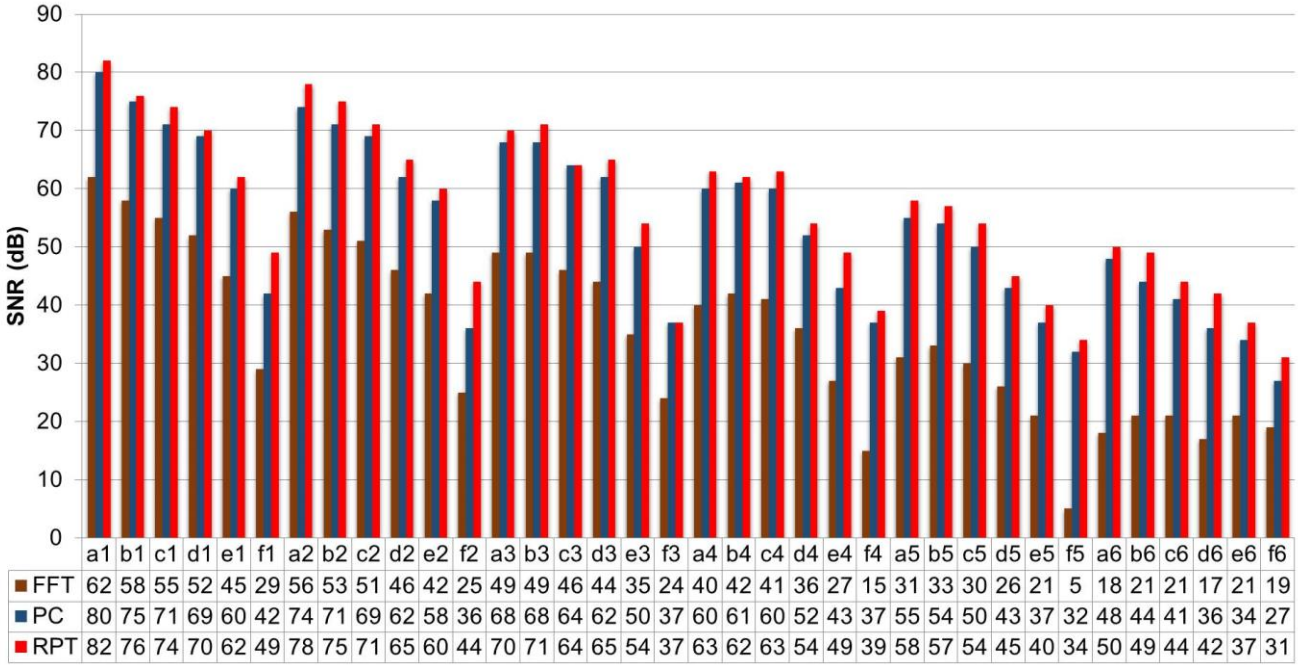

	a1	b1	c1	d1	e1	f1	a2	b2	c2	d2	e2	f2	a3	b3	c3	d3	e3	f3	a4	b4	c4	d4	e4	f4	a5	b5	c5	d5	e5	f5	a6	b6	c6	d6	e6	f6
FFT	62	58	55	52	45	29	56	53	51	46	42	25	49	49	46	44	35	24	40	42	41	36	27	15	31	33	30	26	21	5	18	21	21	17	21	19
PC	80	75	71	69	60	42	74	71	69	62	58	36	68	68	64	62	50	37	60	61	60	52	43	37	55	54	50	43	37	32	48	44	41	36	34	27
RPT	82	76	74	70	62	49	78	75	71	65	60	44	70	71	64	65	54	37	63	62	63	54	49	39	58	57	54	45	40	34	50	49	44	42	37	31

Fig. 6 Comparison of SNR of defects for processed results of FFT, PC and RPT

5- Conclusions

The defect detection capability of QFMTWI through enhanced depth resolution was explored by experimenting with CFRP sample. The projection of randomly generated orthonormal vectors on the thermal response discriminates the deeper and smaller defects with fine contrast. RPT based post-processing technique is validated by comparing the processed results of RPT with conventional FFT and PC based post-processing approaches in terms of SNR and FWHM. The obtained results are evident for the estimation of defect sizing by applying full width at half maxima with an error

percentage of 0.99% for deeper and smaller defects. SNR is also considered to further validate the potentiality of detecting the defects and it is measured as minimum of 31dB. Based on the above validation parameters the analysis dependent on RPT technique holds by experimentation is achieved with enhanced detectability, estimation of defect size & evaluation of the subsurface anomalies qualitatively by employing 3D green's function based analytical approach using QFMTWI.

Acknowledgments

This work was partially supported by Naval Research Board, India grant no: NRB-423/MAT/18-19 and FIST sponsored ECE Department under grant no. SR/FST/ET-II/2019/450.

Table 1: Comparison of FWHM of defects of the last column for processed results of FFT phase, PC and RPT

Defect	*Actual defect size (cm)*	*Estimated size (cm)*					
		FFT phase	*% of error*	*PC*	*% of error*	*RPT*	*% of error*
a_1	1.6	1.47	8.84	1.48	8.11	1.605	0.31
a_2	1.4	1.45	3.45	1.43	2.10	1.41	0.71
a_3	1.2	1.09	10.09	1.14	5.26	1.195	0.42
a_4	1.0	0.95	5.26	0.96	4.17	1.01	0.99
a_5	0.8	0.71	12.68	0.73	9.59	0.805	0.62
a_6	0.6	0.46	30.43	0.51	17.65	0.596	0.67

References

[1] X. Maldague, Theory and practice of infrared technology for nondestructive testing, New York: Wiley, 2001.

[2] H. Benítez, C. Ibarra-Castanedo, A. Bendada, X. Maldague, H. Loaiza, and E. Caicedo, "Definition of a new thermal contrast and pulse correction for defect quantification in pulsed thermography", Infrared Physics & Technology, Vol. 51, No. 3, 2008, pp. 160-167.

[3] A. Castelo, A. Mendioroz, R. Celorrio, and A. Salazar, "Optimizing the Inversion Protocol to Determine the Geometry of Vertical Cracks from Lock-in Vibrothermography", Journal of Nondestructive Evaluation, Vol. 36, No. 1, 2016.

[4] C. Ibarra-Castanedo, N. Avdelidis, and X. Maldague, "Quantitative pulsed phase thermography applied to steel plates", Thermosense XXVII, 2005.

[5] R. Mulaveesala, and S. Tuli, "Theory of frequency modulated thermal wave imaging for nondestructive subsurface defect detection", Applied Physics Letters, Vol. 89, No. 19, 2006, p. 191913.

[6] G. V. Subbarao, and R. Mulaveesala, "Quadratic Frequency Modulated Thermal Wave Imaging for Non-Destructive Testing", Progress In Electromagnetics Research M, Vol. 26, 2012, pp. 11-22.

[7] B. Suresh, S. Subhani, A. Vijayalakshmi, V. Vardhan, and V. S. Ghali, "Chirp Z transform based enhanced frequency resolution for depth resolvable non stationary thermal wave imaging", Review of Scientific Instruments, Vol. 88, No. 1, 2017, p. 014901.

[8] A. Sharma, R. Mulaveesala, and V. Arora, "Novel Analytical Approach for Estimation of Thermal Diffusivity and Effusivity for Detection of Osteoporosis", IEEE Sens. J., Vol.20, No. 11, 2020, pp. 6046–6054.

[9] V. S. Ghali, S. Panda, and R. Mulaveesala, "Barker coded thermal wave imaging for defect detection in carbon fibre-reinforced plastics", Insight - Non-Destructive Testing and Condition Monitoring, Vol. 53, No. 11, 2011, pp. 621-624.

[10] B. Suresh, S. Subhani, V. S. Ghali, and R. Mulaveesala, "Subsurface detail fusion for anomaly detection in non-stationary thermal wave imaging", Insight - Non-Destructive Testing and Condition Monitoring, Vol. 59, No. 10, 2017, pp. 553-558.

[11] G.V.P. Chandra Sekhar Yadav, V. S. Ghali, B. Sonali Reddy, B. Omprakash, and Ch. Chaitanya Reddy, "Greens Function Based Analytical Model for Enhanced Defect Detection Using Depth Resolvable Non-Stationary Thermal Wave Imaging", Journal of Green Engineering, Vol. 10, No. 12, 2020, pp. 12933-12947.

[12] S. Subhani, and V. S. Ghali, "Measurement of thermal diffusivity of fiber reinforced polymers using quadratic frequency modulated thermal wave imaging", Infrared Physics & Technology, Vol. 99, 2019, pp. 187-192.

[13] S. Subhani, B. Suresh, and V. S. Ghali, "Quantitative subsurface analysis using frequency modulated thermal wave imaging", Infrared Physics & Technology, Vol. 88, 2018, pp. 41-47.

[14] M. Pasha, B. Suresh, K. Rajesh Babu, S. Subhani, and G. V. Subbarao, "Barker coded modulated thermal wave imaging for defect detection of glass fiber reinforced plastic", ARPN Journal of Engineering and Applied Sciences, Vol. 13, No. 10, 2018, pp. 3475-3480.

[15] G.V.P. Chandra Sekhar Yadav, V. Ghali, and N. Baloji, "A Time Frequency-Based Approach for Defect Detection in Composites Using Nonstationary Thermal Wave Imaging", Russian Journal of Nondestructive Testing, Vol. 57, No. 6, 2021, pp. 486-499.

[16] M. Pasha, G. V. Subbarao, B. Suresh, and S. Tabassum, "Inspection of Defects in CFRP based on Principal Components", International Journal of Recent Technology and Engineering, Vol. 8, No. 3, 2019, pp. 2367-2370.

[17] V. S. Ghali, B. Suresh, and A. Hemanth, "Data Fusion for Enhanced Defect Detectability in Non-Stationary Thermal Wave Imaging", IEEE Sensors Journal, Vol. 15, No. 12, 2015, pp. 6761-6762.

[18] B. Suresh, J. Sai kiran, and G. V. Subbarao, "Automatic detection of subsurface anomalies using non-linear chirped thermography", International Journal of Innovative Technology and Exploring Engineering, Vol. 8, No. 6, 2019, pp. 1247-1249.

[19] M. Parvez M, J. Shanmugam, and V. S. Ghali, "Decision tree-based subsurface analysis using Barker coded thermal wave imaging", Infrared Physics & Technology, Vol. 109, 2020, p. 103380.

[20] A. Vijaya Lakshmi, V. Gopitilak, M. Parvez, S. Subhani, and V. S. Ghali, "Artificial neural networks based quantitative evaluation of subsurface anomalies in quadratic frequency modulated thermal wave imaging", Infrared Physics & Technology, Vol. 97, 2019, pp. 108-115.

[21] S. Subhani, G. V. P. Chandra Sekhar Yadav, and V. S. Ghali, "Defect characterisation using pulse compression-based quadratic frequency modulated thermal wave imaging", IET Science, Measurement & Technology, Vol. 14, No. 2, 2020, pp. 165-172.

[22] B. Suresh, M. Manorama, M. Bhupesh, K. Sai Kiran, G. V. P. Chandra Sekhar Yadav, and V. S. Ghali, "Advanced Signal Processing Approaches for Quadratic Frequency Modulated Thermal Wave Imaging", International Journal of Emerging Trends in Engineering Research, Vol. 7, No. 11, 2019, pp. 599-603.

[23] S. Subhani, B. Suresh, and V. S. Ghali, "Orthonormal projection approach for depth-resolvable subsurface analysis in non-stationary thermal wave imaging", Insight - Non-Destructive Testing and Condition Monitoring, Vol. 58, No. 1, 2016, pp. 42-45.

[24] A. Vijaya Lakshmi, K. Nagendra Babu, M. Sree Ram Deepak, A. Sai Kumar, G. V. P. Chandra Sekhar Yadav, V. Gopi Tilak, and V. S. Ghali, "A Machine Learning based Approach for Defect Detection and Characterization in Non-Linear Frequency Modulated Thermal Wave Imaging", International Journal of Emerging Trends in Engineering Research, Vol. 7, No. 11, 2019, pp. 517-522.

[25] A. Vijaya Lakshmi, V. S. Ghali, M. Parvez, G. V. P. Chandra Sekhar Yadav, and V. Gopi Tilak, "Fuzzy C-Means Clustering Based Anomalies Detection in Quadratic Frequency Modulated Thermal Wave Imaging", International Journal of Recent Technology and Engineering, Vol. 8, No. 3, 2019, pp. 4047-4051.

[26] A. Vijaya Lakshmi, V. S. Ghali, S. Subhani, and N. Baloji, "Automated quantitative subsurface evaluation of fiber reinforced polymers", Infrared Physics & Technology, Vol. 110, 2020, p. 103456.